Study of $B_s^0 \to TT(a_2(1320), K_2^*(1430), f_2(1270), f_2'(1525))$ in the perturbative QCD approach

Jing Dai[*] and Xian-Qiao Yu[†]

School of Physical Science and Technology, Southwest University, Chongqing 400715, China

In the present study, the calculations of two-body decays $B_s^0 \to TT$ [T denotes tensor mesons, $a_2(1320)$, $K_2^*(1430)$, $f_2(1270)$, $f_2'(1525)$] in the perturbative QCD approach are presented. The ensuing predictions encompass branching ratios, polarization fractions, and direct CP violations, all elucidated in comprehensive detail. It is discerned that (1) for pure annihilation decay, the longitudinal polarization is around 90.0%, whereas the transverse polarizations manifest comparatively diminutive magnitudes. (2) The direct CP asymmetry is directly proportional to the interference between the tree and penguin contributions. For most of the decays investigated within this discourse, the direct CP asymmetry remains modest in magnitude. (3) There are precisely six distinct categories of Feynman diagrams for $B_s^0 \to TT$, because the tensor mesons cannot be produced through the $(V \pm A)$ currents or $(S \pm P)$ density, thereby prohibiting factorizable emission diagrams. The nonfactorizable and annihilation contributions are ascertained to be pivotal in these decay modes. The calculated branching ratios of our calculation for $B_s^0 \to TT$ are at the order of 10^{-6} and 10^{-7}, which can be tested in the LHCb and Belle II experiments. (4) Mixing exists for the $f_2(1270)$ and $f_2'(1525)$, just as the η and η' mixing, the branching ratios about the mixing angle θ are given in this work. However, it is different from $f_1(1285) - f_1(1420)$, the mixing angle is notably small, thereby resulting in only marginal alterations in the decay branching ratios.

I. INTRODUCTION

The model elucidating the two-body decay of B mesons has been the subject of extensive scrutiny over the past two decades, both from a theoretical [1–4] and experimental [5–7] perspective. The emergence of charmless hadronic B decays featuring a light tensor meson in the final state has invigorated interest in tensor mesons. Based on the principles of flavor SU(3) symmetry, we investigate nine mesons [8,9], comprising isovector mesons $a_2(1320)$, isodoulet states $K_2^*(1430)$, and two isosinglet mesons $f_2(1270)$, $f_2'(1525)$, which forms the first 1^3P_2 nonet [10]. According to the latest experimental data of 2022 PDG [8], the $B_s^0 \to K_2^*(1430)\bar{K}_2^*(1430)$ decay has already appeared, signifying the emergence of numerous decay modes involving the final state of two tensor mesons may appear. In Ref. [2], some researchers have calculated the decay channel about $B_s^0 \to VT$, at the same time, they also adopted some other methods to compare. Further, these calculations indicated that predictions based on the pQCD

that can accommodate experimental data well. By comparing their predictions with the experimental data, we find that $\mathcal{BR}(B_s^0 \to \Phi(K_2^*(1430), \bar{K}_2^*(1430)))$ is similar to $\mathcal{BR}(B_s^0 \to \Phi(K^*(1430), \bar{K}^*(1430)))$, but the magnitude is smaller. For $B_s^0 \to VV, TV$, they are similar but a little different.

In the exploration of two-body decay of B mesons, the perturbative QCD factorization approach assumes paramount significance. This method based on factorization [11–17] to calculate the decay process of $B_s^0 \to M_1 M_2$, in which M_i are composed of light noncharmed mesons. In the perturbative QCD framework, the factorization scale about $1/b$ is employed to demarcate the boundary between the perturbative and nonperturbative regimes. The nonleptonic decay of the B meson is postulated to be primarily governed by the exchange of hard gluons, permitting the isolation and direct computation of the hard portion of the decay process through perturbative methodologies. Simultaneously, the nonperturbative component is absorbed into the universal hadron wave function. On this foundation, the two-body decay amplitude of B_s^0 meson is generically expressed as

$$\mathcal{A} = \mathcal{H} \otimes \phi_{B_s^0} \otimes \phi_{h_1} \otimes \phi_{h_2}. \tag{1}$$

Here the hard decay kernel $\mathcal{H}$ represents the contributions emanating from Feynman diagrams, amenable to computation through perturbative theory. The nonperturbative

[*]2446041605@qq.com
[†]yuxq@swu.edu.cn

inputs $\phi_{B_s^0}$, ϕ_{h_1}, and ϕ_{h_2} denote the wave functions of B_s^0 meson, tensor mesons, respectively. These wave functions may be deduced via the extraction of pertinent empirical data or calculated through various nonperturbative methodologies.

Theoretical investigations into the calculations pertaining to tensor mesons have garnered the attention of several researchers. In comparison to vector mesons, tensor mesons are more special and complex. For $B \to PT$, VT [1,18], some scholars have investigated the tensor meson in the final state. However, for $B_s^0 \to TT$, the case where the final states are all tensor mesons has not yet been studied in the literature, and this article is the first in this perspective. For the decays of $B_s^0 \to TT$, the amplitude can be defined as three invariant helicity components: A_0, for which the polarizations of the tensor meson are longitudinal with the respect to their momenta, and $A_\parallel$, $A_\perp$ are for transversely polarized tensor meson [19,20].

The branching ratios of $B_s^0 \to f_2(f_2')f_2(f_2')$ are contingent upon the mixing angle θ of $f_2(1270)$ and $f_2'(1525)$, analogous to η and η' mixing in the pseudoscalar sector [4,21–23]. From the experiment that $\pi\pi$ is the dominant decay mode of $f_2(1270)$, and $f_2'(1525)$ decays dominantly into KK, we can know that the physical $f_2(1270) - f_2'(1525)$ mixing angle is smaller than the decoupling value: $\theta_{T,ph} - \theta_{dec} = 29.5° - 35.26° = -5.8°$ [10,24], which indicates $f_2(1270)$ is nearly $f_2^u + f_2^d$, while $f_2'(1525)$ is mainly f_2^s [25]. The corresponding helicity amplitudes are characterized as follows [26,27]:

$$f_2(1270) = \frac{1}{\sqrt{2}}(f_2^u + f_2^d)\cos\theta_{f_2} - f_2^s\sin\theta_{f_2},$$

$$f_2'(1525) = \frac{1}{\sqrt{2}}(f_2^u + f_2^d)\cos\theta_{f_2} + f_2^s\sin\theta_{f_2}, \quad (2)$$

where $f_2^d = d\bar{d}$, $f_2^u = u\bar{u}$, $f_2^s = s\bar{s}$. Moreover, it is also found that the mixing angle $\theta_{f_2} = 7.8°$ [25] and $(9 \pm 1)°$ [28].

This paper is structured as follows: In Sec. II, we expound upon the theoretical underpinnings of the perturbative QCD (pQCD) framework and elaborate upon the wave functions integral to our calculation for the $B_s^0 \to TT$ decays. Section III assembles the helicity amplitudes. Subsequently, in Sec. IV, we present the numerical results and engage in discussions. The key content of Sec. V comprises a summarization of the principal contributions of this study. Finally, the explicit formulations of all the helicity amplitudes are provided in the Appendix for reference.

II. THEORETICAL FRAMEWORK

A. Hamiltonian and kinematics

The pertinent weak effective Hamiltonian governing the decays $B_s^0 \to TT$ is defined by the following expression [29,30]

$$\mathcal{H}_{\text{eff}} = \frac{G_F}{\sqrt{2}}\left\{V_{ub}^*V_{us}[C_1 O_1 + C_2 O_2] - V_{tb}^*V_{ts}\left[\sum_{i=3}^{10} C_i O_i\right]\right\}, \quad (3)$$

where $V_{ub}^*V_{us}$ and $V_{tb}^*V_{ts}$ are Cabibbo-Kobayashi-Maskawa factors, the Fermi coupling constant $G_F = 1.66378 \times 10^{-5}$ GeV^{-2}, and C_i is the Wilson coefficient corresponding to the quark operator, O_i represents the local four-quark operators, which can be expressed as

$$O_1 = \bar{b}_\alpha\gamma_\mu(1 - \gamma_5)u_\beta\bar{u}_\beta\gamma^\mu(1 - \gamma_5)X_\alpha,$$

$$O_2 = \bar{b}_\alpha\gamma_\mu(1 - \gamma_5)u_\alpha\bar{u}_\beta\gamma^\mu(1 - \gamma_5)X_\beta,$$

$$O_3 = \bar{b}_\alpha\gamma_\mu(1 - \gamma_5)X_\alpha\sum_{X'}\bar{X}'_\beta\gamma^\mu(1 - \gamma_5)X'_\beta,$$

$$O_4 = \bar{b}_\alpha\gamma_\mu(1 - \gamma_5)X_\beta\sum_{X'}\bar{X}'_\beta\gamma^\mu(1 - \gamma_5)X'_\alpha,$$

$$O_5 = \bar{b}_\alpha\gamma_\mu(1 - \gamma_5)X_\alpha\sum_{X'}\bar{X}'_\beta\gamma^\mu(1 + \gamma_5)X'_\beta,$$

$$O_6 = \bar{b}_\alpha\gamma_\mu(1 - \gamma_5)X_\beta\sum_{X'}\bar{X}'_\beta\gamma^\mu(1 + \gamma_5)X'_\alpha,$$

$$O_7 = \frac{3}{2}\bar{b}_\alpha\gamma_\mu(1 - \gamma_5)X_\alpha\sum_{X'}e_{X'}\bar{X}'_\beta\gamma^\mu(1 + \gamma_5)X'_\beta,$$

$$O_8 = \frac{3}{2}\bar{b}_\alpha\gamma_\mu(1 - \gamma_5)X_\beta\sum_{X'}e_{X'}\bar{X}'_\beta\gamma^\mu(1 + \gamma_5)X'_\alpha,$$

$$O_9 = \frac{3}{2}\bar{b}_\alpha\gamma_\mu(1 - \gamma_5)X_\alpha\sum_{X'}e_{X'}\bar{X}'_\beta\gamma^\mu(1 - \gamma_5)X'_\beta,$$

$$O_{10} = \frac{3}{2}\bar{b}_\alpha\gamma_\mu(1 - \gamma_5)X_\beta\sum_{X'}e_{X'}\bar{X}'_\beta\gamma^\mu(1 - \gamma_5)X'_\alpha, \quad (4)$$

where α and β are color indices, $X' = u$, d, s, c, or b quarks, and they are the active quarks at the scale m_b. O_1 and O_2 are current-current operators, $O_i(i = 3, \ldots, 10)$ are penguin operators, in which $O_i(i = 7, \ldots, 10)$ are the electroweak penguin operators. The operators $O_{7\gamma}$ and O_{8g} are not listed, because their contribution is neglected.

Within the framework of the pQCD approach, the decay amplitude can be meticulously into three constituent components: the hard scattering kernel, the wave functions characterizing the mesons, and the convolution of the Wilson coefficients. For $B_s^0 \to M_1 M_2$ decay, the decay amplitude is presented as follows [20,31–33]

$$\mathcal{A} \sim \int dx_1 dx_2 dx_3 b_1 db_1 b_2 db_2 b_3 db_3$$
$$\cdot \text{Tr}[C(t)\Phi_B(x_1, b_1)\Phi_{M_2}(x_2, b_2)\Phi_{M_3}(x_3, b_3)$$
$$\times \mathcal{H}(x_i, b_i, t)S_t(x_i)e^{-S(t)}], \quad (5)$$

where x_i are the proportions of the momenta for the spectator quark inside the mesons B_s^0, T_2, and T_3, respectively, with the values ranging from 0 to 1, b_i are the conjugate space coordinates of the transverse momenta k_i for the light quarks. Tr denotes the trace over all Dirac structure and color indices. $C(t)$ is the short distance Wilson coefficients at the hard scale t. t denotes the largest energy scale of the hard part $\mathcal{H}$. The threshold resummation $S_t(x_i)$ stems from the large double logarithms [34], which can remove the end point singularities. The last term $e^{-S(t)}$ is the Sudakov factor, which can suppress soft dynamics [35].

In the context of the light cone coordinate system, the associated physical quantities are represented as follows. Assuming that the initial state of the meson B_s^0 is stationary, the tensor mesons T_2 and the T_3 move in the direction of the lightlike vector $v = (0, 1, 0_\top)$ and $n = (1, 0, 0_\top)$, respectively. Here we use p_1, p_2, and p_3 to represent the momenta of the mesons B_s^0, T_2, and T_3

$$p_1 = \frac{M_{B_s^0}}{\sqrt{2}}(1, 1, 0_\top),$$
$$p_2 = \frac{M_{B_s^0}}{\sqrt{2}}(1 - r_2^2, r_2^2, 0_\top),$$
$$p_3 = \frac{M_{B_s^0}}{\sqrt{2}}(r_3^2, 1 - r_3^2, 0_\top). \quad (6)$$

Moreover, the momenta of the respective light quarks associated with the mesons B_s^0, T_2, and T_3 are

$$k_1 = \left(0, \frac{M_{B_s^0}}{\sqrt{2}}x_1, k_{1\top}\right),$$
$$k_2 = \left(\frac{M_{B_s^0}}{\sqrt{2}}(1 - r_2^2)x_2, 0, k_{2\top}\right),$$
$$k_3 = \left(0, \frac{M_{B_s^0}}{\sqrt{2}}(1 - r_3^2)x_3, k_{3\top}\right), \quad (7)$$

where $M_{B_s^0}$ represents the mass of the meson B_s^0, and $r_2 = \frac{M_{T_2}}{M_{B_s^0}}$, $r_3 = \frac{M_{T_3}}{M_{B_s^0}}$, M_T is the mass of the tensor meson.

B. Wave functions

1. B meson

The wave function of the meson is expressed as a decomposition of Lorentz structures

$$\int \frac{d^4 z}{(2\pi)^4} e^{ik \cdot z}\langle 0|\bar{b}_\alpha(0)d_\beta(z)|B_s(P_1)\rangle$$
$$= \frac{i}{\sqrt{2N_c}}(\not{p}_1 + M_B)\gamma_5\left[\phi_B(x_1, b_1) + \frac{\not{n}}{\sqrt{2}}\bar{\phi}_B(x_1, b_1)\right], \quad (8)$$

where $\phi_B(x_1, b_1)$ and $\bar{\phi}_B(x_1, b_1)$ are the twist distribution amplitudes, the contribution of $\bar{\phi}_B(x_1, b_1)$ is relatively small, so we neglect it. Therefore, the meson B_s^0 is deemed to be a heavy-light model, with the wave function defined as [36–39]

$$\Phi_B = \frac{i}{\sqrt{2N_c}}(\not{p}_1 + M_B)\gamma_5\phi_B(x_1, b_1), \quad (9)$$

where $N_c = 3$ is the number of colors, because we calculate the relevant parameters in the b space, and the distribution amplitude ϕ_B can be expressed as [40,41]

$$\phi_B(x_1, b_1) = N_B x_1^2(1 - x_1)^2 \exp\left[-\frac{M_B^2 x_1^2}{2\omega_B^2} - \frac{1}{2}(\omega_B b_1)^2\right]. \quad (10)$$

This distribution amplitude adheres to the normalization condition

$$\int_0^1 dx\phi_B(x, b = 0) = \frac{f_B}{2\sqrt{2N_c}}, \quad (11)$$

where $N_B = 91.784$ GeV is the normalization constant, f_B is the decay constant. For B_s^0 meson, we use the shape parameter $\omega_{B_s} = 0.50 \pm 0.05$ GeV [4].

2. Tensor meson

For the spin-2 polarization tensor $\epsilon^{uv}(\lambda)$ with helicity λ, satisfies $\epsilon_{uv}p_2^v = 0$ [42,43], which can be constructed based on the polarization vectors of vector mesons ϵ, they can be written as

$$\epsilon_{uv}(\pm 2) \equiv \epsilon(\pm 1)_u\epsilon(\pm 1)_v,$$
$$\epsilon_{uv}(\pm 1) \equiv \frac{1}{\sqrt{2}}[\epsilon(\pm 1)_u\epsilon(0)_v + \epsilon(0)_u\epsilon(\pm 1)_v],$$
$$\epsilon_{uv}(0) \equiv \frac{1}{\sqrt{6}}[\epsilon(+1)_u\epsilon(-1)_v + \epsilon(-1)_u\epsilon(+1)_v]$$
$$+ \sqrt{\frac{2}{3}}\epsilon(0)_u\epsilon(0)_v. \quad (12)$$

With the tensor meson moving in the plus direction of the z axis, the polarizations ϵ are defined as

$$\epsilon_u(0) = \frac{1}{m_T}(|P_T|, 0, 0, E_T),$$

$$\epsilon_u(\pm 1) = \frac{1}{\sqrt{2}}(0, \pm 1, i, 0), \tag{13}$$

where E_T represents the energy of the tensor meson. In the subsequent calculations, the introduction of a new polarization vector ϵ_T for the tensor meson under consideration is deemed necessary for the sake of convenience [9]

$$\epsilon_{Tu}(\lambda) = \frac{1}{m_B}\epsilon_{uv}(\lambda)P_B^v, \tag{14}$$

which satisfies

$$\epsilon_{Tu}(\pm 2) = 0,$$

$$\epsilon_{Tu}(\pm 1) = \frac{1}{\sqrt{2}m_B}\epsilon(0) \cdot P_B \epsilon_u(\pm 1),$$

$$\epsilon_{Tu}(\pm 0) = \sqrt{\frac{2}{3}}\frac{1}{m_B}\epsilon(0) \cdot P_B \epsilon_u(0). \tag{15}$$

The contraction is evaluated as $\epsilon(0) \cdot P_B/m_B = |\vec{P}_T|/m_T$. It is obvious that the new vector ϵ_T is similar to the ordinary polarization vector ϵ, regardless of the dimensionless constants $\sqrt{\frac{1}{2}}\frac{|\vec{P}_T|}{m_T}$ or $\sqrt{\frac{2}{3}}\frac{|\vec{P}_T|}{m_T}$.

The decay constants of the tensor mesons are defined as [9]

$$\langle T|j_{uv}(0)|0\rangle = f_T m_T^2 \epsilon_{uv}^*,$$

$$\langle T|j_{uv\rho}|0\rangle = -if_T^T m_T(\epsilon_{u\rho}^* P_{2v} - \epsilon_{v\rho}^* P_{2u}). \tag{16}$$

Where the currents are expressed as

$$j_{uv}(0) = \frac{1}{2}[\bar{q}_1(0)\gamma_u i\overleftrightarrow{D}_v q_2(0) + \bar{q}_1(0)\gamma_v i\overleftrightarrow{D}_u q_2(0)],$$

$$j_{uv\rho}^+(0) = \bar{q}_2(0)\sigma_{uv} i\overleftrightarrow{D}_\rho q_1(0), \tag{17}$$

with $\overleftrightarrow{D}_u = \vec{D}_u - \overleftarrow{D}_u$, $\vec{D}_u = \vec{\partial}_u + ig_s A_u^a \lambda^a/2$, and $\overleftarrow{D}_u = \overleftarrow{\partial}_u - ig_s A_u^a \lambda^a/2$, respectively. Here we adopted these decay constants from Ref. [42] that have been calculated in the QCD sum rules [44–46], which can be seen from Table I. We can find that the transverse decay constants are

approximately equal to the longitudinal one for $a_2(1320)$, $f_2(1270)$, but it is different from $K_2^*(1430)$ and $f_2'(1525)$, their ratio relationship: $f_T^T/f_T \sim (50\% - 65\%)$.

From earlier studies [42], we obtain insights into the light cone distribution amplitudes of the tensor mesons. The light cone distribution amplitudes up to twist-3 for generic tensor mesons are defined as follows:

$$\langle T(p_2, \epsilon)|q_{1\alpha}(0)\bar{q}_{2\beta}(z)|0\rangle$$
$$= \frac{1}{\sqrt{2N_c}}\int_0^1 dx e^{ixp_2 \cdot z}\left[m_T \not\epsilon_{\bullet L}^* \Phi_T(x)\right.$$
$$\left. + \not\epsilon_{\bullet L}^* \not p_2 \Phi_T^t(x) + m_T^2 \frac{\epsilon_\bullet \cdot v}{p_2 \cdot v}\Phi_T^s(x)\right]_{\alpha\beta}, \tag{18}$$

$$\langle T(p_2, \epsilon)|q_{1\alpha}(0)\bar{q}_{2\beta}(z)|0\rangle$$
$$= \frac{1}{\sqrt{2N_c}}\int_0^1 dx e^{ixp_2 \cdot z}[m_T \not\epsilon_{\bullet T}^* \Phi_T^v(x)$$
$$+ \not\epsilon_{\bullet T}^* \not p_2 \Phi_T^T(x) + m_T i\epsilon_{uv\rho\sigma}\gamma_5 \gamma^u \epsilon_{\bullet T}^{*v} n^\rho v^\sigma \Phi_T^a(x)]_{\alpha\beta}. \tag{19}$$

The convention $\epsilon^{0123} = 1$ has been adopted. Equation (18) is for the longitudinal polarization($\lambda = 0$), and Eq. (19) is for the transverse polarizations ($\lambda = \pm 1$), respectively. Here n is the moving direction of the tensor meson and v is the opposite direction. The new vector $\epsilon_\bullet$ which plays the same role with the polarization vector ϵ, which is defined by

$$\epsilon_{\bullet u} = \frac{\epsilon_{uv}v^v}{p_2 \cdot v}m_T. \tag{20}$$

With the momenta and polarizations, which can be reexpressed as

$$\epsilon_{\bullet u} = \frac{2m_T}{m_B^2}p_B^v \epsilon_{uv}. \tag{21}$$

In earlier studies [9,42,43], the amplitudes are expressed as

$$\Phi_T(x) = \frac{f_T}{2\sqrt{2N_c}}\Phi_\parallel(x), \quad \Phi_T^t(x) = \frac{f_T^T}{2\sqrt{2N_c}}h_\parallel^{(t)}(x),$$

$$\Phi_T^s(x) = \frac{f_T^T}{4\sqrt{2N_c}}\frac{d}{dx}h_\parallel^s(x), \quad \Phi_T^T(x) = \frac{f_T^T}{2\sqrt{2N_c}}\Phi_\perp(x),$$

$$\Phi_T^v(x) = \frac{f_T}{2\sqrt{2N_c}}g_\perp^v(x), \quad \Phi_T^a(x) = \frac{f_T}{8\sqrt{2N_c}}\frac{d}{dx}g_\perp^a(x). \tag{22}$$

TABLE I. Decay constants (in unit of MeV) of tensor mesons.

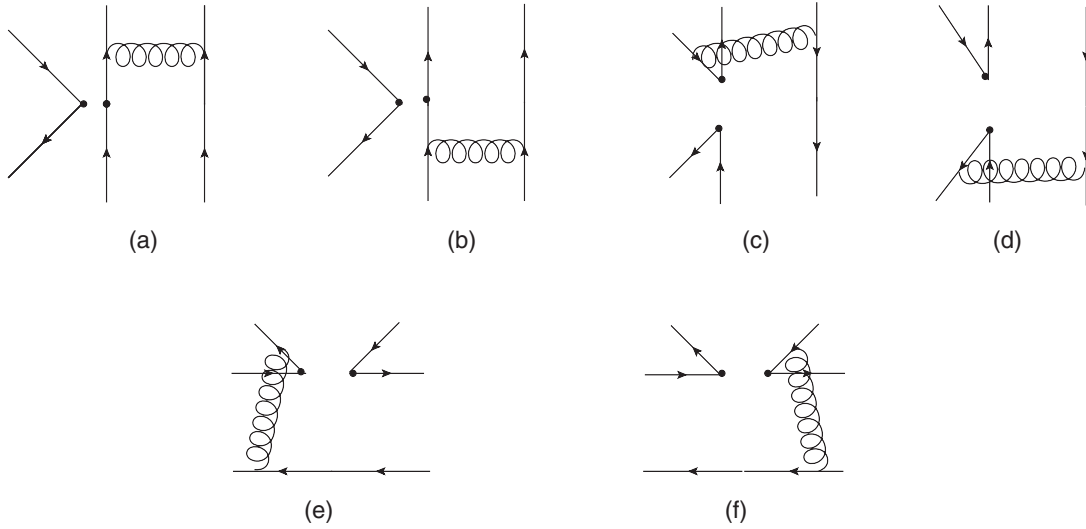|			
$f_{a_2(1320)} = 107 \pm 6$	$f_{K_2^*(1430)} = 118 \pm 5$	$f_{f_2(1270)} = 102 \pm 6$	$f_{f_2'(1525)} = 126 \pm 4$
$f_{a_2(1320)}^T = 105 \pm 21$	$f_{K_2^*(1430)}^T = 77 \pm 14$	$f_{f_2(1270)}^T = 117 \pm 25$	$f_{f_2'(1525)}^T = 65 \pm 12$

FIG. 1. The Feynman diagrams for the $B_s^0 \to TT$ decays. (a) and (b) are factorizable annihilation diagrams, (c) and (d) are the nonfactorizable annihilation diagrams, (e) and (f) are nonfactorizable emission diagrams.

The twist-2 distribution amplitudes can be expanded in terms of Gegenbauer polynomials $C_n^{3/2}(2x-1)$, with the asymptotic form given by

$$\Phi_{\parallel,\perp}(x) = 30x(1-x)(2x-1). \tag{23}$$

Adhering to normalization conditions

$$\int_0^1 dx(2x-1)\Phi_{\parallel,\perp}(x) = 1. \tag{24}$$

The twist-3 distribution amplitudes also assume an asymptotic form, as delineated in [42]

$$
\begin{aligned}
h_\parallel^t(x) &= \frac{15}{2}(2x-1)(1-6x+6x^2), \\
h_\parallel^s(x) &= 15x(1-x)(2x-1), \\
g_\perp^a(x) &= 20x(1-x)(2x-1), \\
g_\perp^v(x) &= 5(2x-1)^3.
\end{aligned}
\tag{25}
$$

III. DECAY AMPLITUDES

In this section, we provide the perturbative QCD formulas for all the Feynman diagrams, as illustrated in Fig. 1. The first row showcases the annihilation-type diagrams, with the first two being factorizable and the last two being nonfactorizable. The second row consists of nonfactorizable emission diagrams. For the $B_s^0 \to TT$ decays, both the longitudinal polarization and the transverse polarization contribute. The symbol F and M represent the factorizable and nonfactorizable contributions, respectively. The superscripts LL denotes the amplitude of the $(V-A)(V-A)$ operators, and LR describe the amplitude of the $(V-A)(V+A)$ operators. The symbol SP is Fierz transformation of LR. Notably, the decay amplitudes for longitudinal and transverse polarizations exhibit the same form after simplification, as follows in Eqs. (26)–(49).

The longitudinal polarization amplitudes of the factorizable annihilation diagrams are

$$
\begin{aligned}
F_{af}^{LL,L} &= \frac{16}{3}\pi C_F f_B M_{B_s^0}^4 \int_0^1 dx_2 dx_3 \int_0^{\frac{1}{\lambda}} b_2 db_2 b_3 db_3 \{[2r_2r_3x_3\phi_T^s(x_2)\phi_T^t(x_3) - 2r_2r_3x_3(x_3-2)\phi_T^s(x_2)\phi_T^s(x_3) \\
&\quad + (x_3-1)\phi_T(x_2)\phi_T(x_3)]E_{af}(t_e)h_{af}(\alpha_1,\beta,b_2,b_3) + [-2r_2r_3(x_2-1)\phi_T^s(x_3)\phi_T^t(x_2) \\
&\quad + 2r_2r_3(-x_2-1)\phi_T^s(x_2)\phi_T^s(x_3) + x_2\phi_T(x_2)\phi_T(x_3)]E_{af}(t_f)h_{af}(\alpha_2,\beta,b_3,b_2)\},
\end{aligned}
\tag{26}
$$

$$
\begin{aligned}
F_{af}^{SP,L} &= -\frac{32}{3}\pi C_F f_B M_{B_s^0}^4 \int_0^1 dx_2 dx_3 \int_0^{\frac{1}{\lambda}} b_2 db_2 b_3 db_3 \{[2r_2\phi_T^s(x_2)\phi_T(x_3) + r_3(x_3-1)\phi_T^s(x_3)\phi_T(x_2) + r_3(x_3-1) \\
&\quad \times \phi_T(x_2)\phi_T^t(x_3)]E_{af}(t_e)h_{af}(\alpha_1,\beta,b_2,b_3) + [2r_3(x_2-1)\phi_T^s(x_3)\phi_T(x_2) + r_2x_2\phi_T^s(x_3)\phi_T^t(x_2) \\
&\quad - r_2x_2\phi_T^s(x_2)\phi_T(x_3)]E_{af}(t_f)h_{af}(\alpha_2,\beta,b_3,b_2)\}.
\end{aligned}
\tag{27}
$$

The longitudinal polarization amplitudes of the nonfactorizable annihilation diagrams are given below

$$
\begin{aligned}
M_{anf}^{LL,L} = \frac{32}{3}\sqrt{\frac{2}{3}}\pi C_F M_{B_s^0}^4 \int_0^1 dx_1 dx_2 dx_3 \int_0^{\frac{1}{\Lambda}} b_1 db_1 b_2 db_2 \phi_{B_s}(x_1, b_1) \\
\times \{[r_2 r_3((1 - x_2 + x_3)\phi_T^t(x_2)\phi_T^t(x_3) + (x_2 + x_3 - 1)\phi_T^t(x_2)\phi_T^s(x_3) \\
+ (1 - x_2 - x_3)\phi_T(x_2)\phi_T(x_3) + (x_2 - x_3 + 3)\phi_T^s(x_2)\phi_T^s(x_3)) \\
- x_2\phi_T(x_2)\phi_T(x_3)]E_{anf}(t_g)h_{anf}(\alpha, \beta_1, b_1, b_2) \\
+ [-r_2 r_3((1 + x_2 - x_3)\phi_T^s(x_2)\phi_T^s(x_3) + (x_2 + x_3 - 1)\phi_T^s(x_2)\phi_T^t(x_3) \\
+ (1 - x_2 - x_3)\phi_T^t(x_2)\phi_T^s(x_3) + (x_3 - x_2 - 1)\phi_T^t(x_2)\phi_T^t(x_3)) \\
+ (x_3 - 1)\phi_T(x_2)\phi_T(x_3)]E_{anf}(t_h)h_{anf}(\alpha, \beta_2, b_1, b_2)\},
\end{aligned}
\tag{28}
$$

$$
\begin{aligned}
M_{anf}^{LR,L} = \frac{32}{3}\sqrt{\frac{2}{3}}\pi C_F M_{B_s^0}^4 \int_0^1 dx_1 dx_2 dx_3 \int_0^{\frac{1}{\Lambda}} b_1 db_1 b_2 db_2 \phi_{B_s}(x_1, b_1) \\
\times \{[r_2(2 - x_2)\phi_T^s(x_2)\phi_T(x_3) + r_2(2 - x_2)\phi_T^t(x_2)\phi_T(x_3) \\
+ r_3(x_3 + 1)\phi_T(x_2)\phi_T^s(x_3) - r_3(x_3 + 1)\phi_T^t(x_3)\phi_T(x_2)]E_{anf}(t_g)h_{anf}(\alpha, \beta_1, b_1, b_2) \\
+ [r_2 x_2(\phi_T^s(x_2)\phi_T(x_3) + \phi_T^t(x_2)\phi_T(x_3)) + r_3(1 - x_3)(\phi_T(x_2)\phi_T^s(x_3) \\
- \phi_T(x_2)\phi_T^t(x_3))]E_{anf}(t_h)h_{anf}(\alpha, \beta_2, b_1, b_2)\},
\end{aligned}
\tag{29}
$$

$$
\begin{aligned}
M_{anf}^{SP,L} = -\frac{32}{3}\sqrt{\frac{2}{3}}\pi C_F f_B M_{B_s^0}^4 \int_0^1 dx_1 dx_2 dx_3 \int_0^{\frac{1}{\Lambda}} b_1 db_1 b_2 db_2 \phi_{B_s}(x_1, b_1) \\
\times \{[r_2 r_3((1 - x_2 + x_3)\phi_T^t(x_2)\phi_T^t(x_3) - (x_2 + x_3 - 1)\phi_T^t(x_2)\phi_T^s(x_3) \\
+ (x_2 + x_3 - 1)\phi_T^s(x_2)\phi_T^t(x_3) + (x_2 - x_3 + 3)\phi_T^s(x_2)\phi_T^s(x_3) \\
+ (x_3 - 1)\phi_T(x_2)\phi_T(x_3)]E_{anf}(t_g)h_{anf}(\alpha, \beta_1, b_1, b_2) \\
- [r_2 r_3((1 + x_2 - x_3)\phi_T^s(x_2)\phi_T^s(x_3) + (1 - x_2 - x_3)\phi_T^s(x_2)\phi_T^t(x_3) + (x_2 + x_3 - 1)\phi_T^t(x_2)\phi_T^s(x_3) \\
+ (x_3 - x_2 - 1)\phi_T^t(x_2)\phi_T^t(x_3)) - x_2\phi_T(x_2)\phi_T(x_3)]E_{anf}(t_h)h_{anf}(\alpha, \beta_2, b_1, b_2)\}.
\end{aligned}
\tag{30}
$$

The longitudinal polarization amplitudes of the nonfactorizable emission diagrams are as follows:

$$
\begin{aligned}
M_{enf}^{LL,L} = -\frac{32}{3}\sqrt{\frac{2}{3}}\pi C_F M_{B_s^0}^4 \int_0^1 dx_1 dx_2 dx_3 \int_0^{\frac{1}{\Lambda}} b_1 db_1 b_2 db_2 \phi_{B_s}(x_1, b_1)\phi_2(x_2) \\
\times \{[(x_2 - 1)\phi_T(x_3) + r_3(x_3 - 1)\phi_T^s(x_3) - r_3(x_3 - 1)\phi_T^t(x_3)]E_{enf}(t_c)h_{enf}(\alpha, \beta_1, b_1, b_2) \\
+ [(x_2 + x_3 - 2)\phi_T(x_3) - r_3(x_3 - 1)\phi_T^s(x_3) - r_3(x_3 - 1)\phi_T^t(x_3)]E_{enf}(t_d)h_{enf}(\alpha, \beta_2, b_1, b_2)\},
\end{aligned}
\tag{31}
$$

$$
\begin{aligned}
M_{enf}^{LR,L} = \frac{32}{3}\sqrt{\frac{2}{3}}\pi C_F M_{B_s^0}^4 r_2 \int_0^1 dx_1 dx_2 dx_3 \int_0^{\frac{1}{\Lambda}} b_1 db_1 b_2 db_2 \phi_{B_s}(x_1, b_1) \\
\times \{[r_3(x_2 - x_3 - 1)(\phi_T^s(x_2)\phi_T^s(x_3) - \phi_T^t(x_2)\phi_T^t(x_3)) + (x_2 + x_3 - 1)(\phi_T^s(x_3)\phi_T^t(x_2) - \phi_T^s(x_2)\phi_T^s(x_3)) \\
+ (x_2 - 1)(\phi_T(x_3)\phi_T^s(x_2) - \phi_T(x_3)\phi_T^t(x_2))]E_{enf}(t_c)h_{enf}(\alpha, \beta_1, b_1, b_2) \\
+ [r_3(x_3 - x_2)(\phi_T^t(x_2)\phi_T^s(x_3) + \phi_T^s(x_2)\phi_T^t(x_3)) + (x_2 + x_3)(\phi_T^s(x_2)\phi_T^s(x_3) + \phi_T^t(x_2)\phi_T^t(x_3)) \\
+ x_2(\phi_T(x_3)\phi_T^s(x_2) - \phi_T(x_3)\phi_T^t(x_2))]E_{enf}(t_d)h_{enf}(\alpha, \beta_2, b_1, b_2)\},
\end{aligned}
\tag{32}
$$

$$M_{enf}^{SP,L} = -\frac{32}{3}\sqrt{\frac{2}{3}}\pi C_F M_{B_s^0}^4 \int_0^1 dx_1 dx_2 dx_3 \int_0^{\frac{1}{\Lambda}} b_1 db_1 b_2 db_2 \phi_{B_s}(x_1, b_1)\phi_2(x_2)$$
$$\times \{[(x_2 - x_3 - 1)\phi_T(x_3) + r_3 x_3 \phi_T^s(x_3) + r_3 x_3 \phi_T^t(x_3)]E_{enf}(t_c)h_{enf}(\alpha, \beta_1, b_1, b_2)$$
$$+ [-r_3 x_3 \phi_T^s(x_3) + r_3 x_3 \phi_T^t(x_3) + x_2 \phi_T(x_3)]E_{enf}(t_d)h_{enf}(\alpha, \beta_2, b_1, b_2)\}. \tag{33}$$

The transverse polarization amplitudes of the factorizable annihilation diagrams are

$$F_{af}^{LL(LR),N} = 4\pi C_F f_B M_{B_s^0}^4 r_2 r_3 \int_0^1 dx_2 dx_3 \int_0^{\frac{1}{\Lambda}} b_2 db_2 b_3 db_3 \{[(x_3 - 2)(\phi_T^v(x_2)\phi_T^v(x_3) + \phi_T^a(x_2)\phi_T^a(x_3)) - x_3 \phi_T^v(x_2)\phi_T^v(x_3)$$
$$- x_3 \phi_T^a(x_2)\phi_T^v(x_3)]E_{af}(t_e)h_{af}(\alpha_1, \beta, b_2, b_3) + [(x_2 - 1)\phi_T^v(x_3)\phi_T^a(x_2) + (x_2 - 1)\phi_T^a(x_3)\phi_T^v(x_2)$$
$$+ (x_2 + 1)\phi_T^a(x_3)\phi_T^a(x_2) + (x_2 + 1)\phi_T^v(x_3)\phi_T^v(x_2)]E_{af}(t_f)h_{af}(\alpha_2, \beta, b_3, b_2)\}, \tag{34}$$

$$F_{af}^{SP,N} = 8\pi C_F f_B M_{B_s^0}^4 \int_0^1 dx_2 dx_3 \int_0^{\frac{1}{\Lambda}} b_2 db_2 b_3 db_3 \{[r_2 \phi_T^a(x_2)\phi_T^T(x_3) + r_2 \phi_T^v(x_2)\phi_T^T(x_3)]E_{af}(t_e)h_{af}(\alpha_1, \beta, b_2, b_3)$$
$$- [r_3 \phi_T^a(x_3)\phi_T^T(x_2) + r_3 \phi_T^v(x_3)\phi_T^T(x_2)]E_{af}(t_f)h_{af}(\alpha_2, \beta, b_3, b_2)\}, \tag{35}$$

$$F_{af}^{LL,T} = 4\pi C_F f_B M_{B_s^0}^4 r_2 r_3 \int_0^1 dx_2 dx_3 \int_0^{\frac{1}{\Lambda}} b_2 db_2 b_3 db_3 \phi_{B_s}(x_1, b_1)$$
$$\times \{[(x_3 - 2)(\phi_T^a(x_2)\phi_T^v(x_3) + \phi_T^v(x_2)\phi_T^a(x_3)) - x_3 \phi_T^v(x_2)\phi_T^a(x_3)$$
$$- x_3 \phi_T^a(x_2)\phi_T^v(x_3)]E_{af}(t_e)h_{af}(\alpha_1, \beta, b_2, b_3) + [(x_2 - 1)\phi_T^v(x_3)\phi_T^v(x_2) + (x_2 - 1)\phi_T^a(x_3)\phi_T^a(x_2)$$
$$+ (x_2 + 1)\phi_T^a(x_3)\phi_T^v(x_2) + (x_2 + 1)\phi_T^v(x_3)\phi_T^a(x_2)]E_{af}(t_f)h_{af}(\alpha_2, \beta, b_3, b_2)\}, \tag{36}$$

$$F_{af}^{SP,N} = -F_{af}^{SP,T}, \tag{37}$$

$$F_{af}^{LL,T} = -F_{af}^{LR,T}. \tag{38}$$

The transverse polarization amplitudes of the nonfactorizable annihilation diagrams are

$$M_{anf}^{LL(SP),N} = 8\sqrt{\frac{2}{3}}\pi C_F M_{B_s^0}^4 \int_0^1 dx_1 dx_2 dx_3 \int_0^{\frac{1}{\Lambda}} b_1 db_1 b_2 db_2 \phi_{B_s}(x_1, b_1)$$
$$\times \{[-2r_2 r_3 \phi_T^a(x_2)\phi_T^a(x_3) - 2r_2 r_3 \phi_T^v(x_2)\phi_T^v(x_3)$$
$$- r_2^2(x_2 - 1)\phi_T^T(x_2)\phi_T^T(x_3) + r_3^2 x_3 \phi_T^T(x_2)\phi_T^T(x_3)]E_{anf}(t_g)h_{anf}(\alpha, \beta_1, b_1, b_2)$$
$$+ [r_2^2 x_2 \phi_T^T(x_2)\phi_T^T(x_3) - r_3^2(x_3 - 1)\phi_T^T(x_2)\phi_T^T(x_3)]E_{anf}(t_h)h_{anf}(\alpha, \beta_2, b_1, b_2)\}, \tag{39}$$

$$M_{anf}^{LR,N} = 8\sqrt{\frac{2}{3}}\pi C_F M_{B_s^0}^4 \int_0^1 dx_1 dx_2 dx_3 \int_0^{\frac{1}{\Lambda}} b_1 db_1 b_2 db_2 \phi_{B_s}(x_1, b_1)$$
$$\times \{[r_2(x_2 - 2)\phi_T^a(x_2)\phi_T^T(x_3) + r_2(x_2 - 2)\phi_T^v(x_2)\phi_T^T(x_3)$$
$$- r_3(x_3 + 1)\phi_T^T(x_2)\phi_T^a(x_2) + r_3(x_3 + 1)\phi_T^T(x_2)\phi_T^v(x_3)]E_{anf}(t_g)h_{anf}(\alpha, \beta_1, b_1, b_2)$$
$$+ [r_3(x_3 - 1)\phi_T^T(x_2)\phi_T^v(x_3) - r_3(x_3 - 1)\phi_T^T(x_2)\phi_T^v(x_3) + r_2 x_2 \phi_T^T(x_3)\phi_T^a(x_2)$$
$$+ r_2 x_2 \phi_T^T(x_3)\phi_T^v(x_2)]E_{anf}(t_h)h_{anf}(\alpha, \beta_2, b_1, b_2)\}, \tag{40}$$

$$M_{anf}^{LR,N} = -M_{anf}^{LR,T}, \tag{41}$$

$$M_{anf}^{LL,T} = 8\sqrt{\frac{2}{3}}\pi C_F M_{B_s^0}^4 \int_0^1 dx_1 dx_2 dx_3 \int_0^{\frac{1}{\Lambda}} b_1 db_1 b_2 db_2 \phi_{B_s}(x_1, b_1)$$
$$\times \{[2r_2 r_3 \phi_T^a(x_2)\phi_T^v(x_3) + 2r_2 r_3 \phi_T^v(x_2)\phi_T^a(x_3)$$
$$- r_2^2(x_2 - 1)\phi_T^T(x_2)\phi_T^T(x_3) - r_3^2 x_3 \phi_T^T(x_2)\phi_T^T(x_3)]E_{anf}(t_g)h_{anf}(\alpha, \beta_1, b_1, b_2)$$
$$+ [r_2^2 x_2 \phi_T^T(x_2)\phi_T^T(x_3) + r_3^2(x_3 - 1)\phi_T^T(x_2)\phi_T^T(x_3)]E_{anf}(t_h)h_{anf}(\alpha, \beta_2, b_1, b_2)\}, \tag{42}$$

$$M_{anf}^{LL,T} = -M_{anf}^{SP,T}. \tag{43}$$

For $B_s^0 \to TT$ decays, the transverse polarization amplitudes of the nonfactorizable emission diagrams are as follows:

$$M_{enf}^{LL,N} = 8\sqrt{\frac{2}{3}}\pi C_F M_{B_s^0}^4 r_2 \int_0^1 dx_1 dx_2 dx_3 \int_0^{\frac{1}{\Lambda}} b_1 db_1 b_2 db_2 \phi_{B_s}(x_1, b_1)$$
$$\times \{[(1 - x_2)\phi_T^a(x_2)\phi_T^T(x_3) + (1 - x_2)\phi_T^T(x_3)\phi_T^v(x_2)]E_{enf}(t_c)h_{enf}(\alpha, \beta_1, b_1, b_2)$$
$$- [2r_3(x_2 + x_3)\phi_T^a(x_2)\phi_T^a(x_3) + 2r_3(x_2 + x_3)\phi_T^v(x_2)\phi_T^v(x_3) - x_2(\phi_T^T(x_3)\phi_T^a(x_2)$$
$$+ \phi_T^T(x_3)\phi_T^v(x_2))]E_{enf}(t_d)h_{enf}(\alpha, \beta_2, b_1, b_2)\}, \tag{44}$$

$$M_{enf}^{LR,N} = 8\sqrt{\frac{2}{3}}\pi C_F M_{B_s^0}^4 \int_0^1 dx_1 dx_2 dx_3 \int_0^{\frac{1}{\Lambda}} b_1 db_1 b_2 db_2 \phi_{B_s}(x_1, b_1)\phi_T^T(x_2)$$
$$\times \{[r_3 x_3 \phi_T^a(x_3) - r_3 x_3 \phi_T^v(x_3) - r_2^2(x_2 - 1)\phi_T^T(x_3) + x_3 r_3^2 \phi_T^T(x_3)]E_{enf}(t_c)h_{enf}(\alpha, \beta_1, b_1, b_2)$$
$$+ [r_3 x_3 \phi_T^a(x_3) - r_3 x_3 \phi_T^v(x_3) + r_2^2 x_2 \phi_T^T(x_3) + x_3 r_3^2 \phi_T^T(x_3)]E_{enf}(t_d)h_{enf}(\alpha, \beta_2, b_1, b_2)\}, \tag{45}$$

$$M_{enf}^{SP,N} = 8\sqrt{\frac{2}{3}}\pi C_F M_{B_s^0}^4 r_2 \int_0^1 dx_1 dx_2 dx_3 \int_0^{\frac{1}{\Lambda}} b_1 db_1 b_2 db_2 \phi_{B_s}(x_1, b_1)$$
$$\times \{[2r_3(x_3 - x_2 + 1)\phi_T^v(x_2)\phi_T^v(x_3) - 2r_3(x_3 + 1 - x_2)\phi_T^a(x_2)\phi_T^a(x_3)$$
$$+ (x_2 - 1)\phi_T^T(x_3)\phi_T^v(x_2) - (x_2 - 1)\phi_T^T(x_3)\phi_T^a(x_2)]E_{enf}(t_c)h_{enf}(\alpha, \beta_1, b_1, b_2)$$
$$+ [x_2 \phi_T^T(x_3)\phi_T^a(x_2) - x_2 \phi_T^v(x_2)\phi_T^T(x_3)]E_{enf}(t_d)h_{enf}(\alpha, \beta_2, b_1, b_2)\}, \tag{46}$$

$$M_{enf}^{LL,T} = 8\sqrt{\frac{2}{3}}\pi C_F M_{B_s^0}^4 r_2 \int_0^1 dx_1 dx_2 dx_3 \int_0^{\frac{1}{\Lambda}} b_1 db_1 b_2 db_2 \phi_{B_s}(x_1, b_1)$$
$$\times \{[(x_2 - 1)\phi_T^a(x_2)\phi_T^T(x_3) + (x_2 - 1)\phi_T^T(x_2)\phi_T^v(x_3)]E_{enf}(t_c)h_{enf}(\alpha, \beta_1, b_1, b_2)$$
$$+ [2r_3(x_2 + x_3)\phi_T^a(x_2)\phi_T^v(x_3) + 2r_3(x_2 + x_3)\phi_T^v(x_2)\phi_T^a(x_3) - x_2\phi_T^T(x_3)\phi_T^a(x_2)$$
$$- x_2\phi_T^T(x_3)\phi_T^v(x_2)]E_{enf}(t_d)h_{enf}(\alpha, \beta_2, b_1, b_2)\}, \tag{47}$$

$$M_{enf}^{LR,T} = 8\sqrt{\frac{2}{3}}\pi C_F M_{B_s^0}^4 \int_0^1 dx_1 dx_2 dx_3 \int_0^{\frac{1}{\Lambda}} b_1 db_1 b_2 db_2 \phi_{B_s}(x_1, b_1)\phi_T^T(x_2)$$
$$\times \{[r_3 x_3 \phi_T^v(x_3) - r_3 x_3 \phi_T^a(x_3) - r_2^2(x_2 - 1)\phi_T^T(x_3) - x_3 r_3^2 \phi_T^T(x_3)]E_{enf}(t_c)h_{enf}(\alpha, \beta_1, b_1, b_2)$$
$$+ [r_3 x_3 \phi_T^v(x_3) - r_3 x_3 \phi_T^a(x_3) + r_2^2 x_2 \phi_T^T(x_3) - x_3 r_3^2 \phi_T^T(x_3)]E_{enf}(t_d)h_{enf}(\alpha, \beta_2, b_1, b_2)\}, \tag{48}$$

$$M_{enf}^{SP,T} = 8\sqrt{\frac{2}{3}}\pi C_F M_{B_s^0}^4 r_2 \int_0^1 dx_1 dx_2 dx_3 \int_0^{\frac{1}{\Lambda}} b_1 db_1 b_2 db_2 \phi_{B_s}(x_1, b_1)$$
$$\times \{[2r_3(x_2 - x_3 - 1)\phi_T^v(x_2)\phi_T^a(x_3) - 2r_3(x_3 + 1 - x_2)\phi_T^a(x_2)\phi_T^v(x_3)$$
$$+ (x_2 - 1)\phi_T^T(x_3)\phi_T^a(x_2) - (x_2 - 1)\phi_T^T(x_3)\phi_T^v(x_2)]E_{enf}(t_c)h_{enf}(\alpha, \beta_1, b_1, b_2)$$
$$+ [x_2\phi_T^T(x_3)\phi_T^v(x_2) - x_2\phi_T^a(x_2)\phi_T^T(x_3)]E_{enf}(t_d)h_{enf}(\alpha, \beta_2, b_1, b_2)\}. \tag{49}$$

TABLE II.   Various parameters involved in the calculation process.

Mass of mesons	$M_{B_s^0} = 5.367$ GeV	$M_{a_2(1320)} = 1.317$ GeV	$M_{K_2^{*0}(1430)} = 1.432$ GeV
	$M_{K_2^{*\pm}(1430)} = 1.427$ GeV	$M_{f_2'(1525)} = 1.517$ GeV	$M_{f_2(1270)} = 1.275$ GeV
	$m_b = 4.18$ GeV	$m_s = 0.093$ GeV	
Decay constants of mesons	$f_{B_s^0} = 0.24 \pm 0.02$ GeV		
Lifetime of meson	$\tau_{B_s^0} = 1.509$ ps		
Wolfenstein parameters	$A = 0.836 \pm 0.015$	$\lambda = 0.22453 \pm 0.00044$	
	$\bar{\eta} = 0.355^{+0.012}_{-0.011}$	$\bar{\rho} = 0.122^{+0.018}_{-0.017}$	

IV. NUMERICAL RESULTS AND DISCUSSIONS

In this section, we initiate our calculations by enumerating the input parameters. These encompass the decay constant f_B, the Wolfenstein parameters, the masses of B meson and tensor mesons, and the corresponding lifetime, as detailed in Table II [47].

Our numerical calculations within the pQCD framework are focused on branching ratios, direct CP violations, and polarization fractions, as summarized in Tables III–V. It is crucial to acknowledge that there exist uncertainties in our calculation results. In Table III, the errors stem from induced by the uncertainties in the shape parameter $\omega_B = (0.50 \pm 0.05)$ GeV pertaining to the B_s^0 meson distribution amplitude [4]. The second source of uncertainty pertains to the B_s^0 meson and the final state tensor mesons, as documented in Table I. The third error arises from $\Lambda_{\mathrm{QCD}} = (0.25 \pm 0.05)$ GeV, and varies 20% from hard scale $t_{\max} = (1.0 \pm 0.2)t$ detailed in the Appendix. Other uncertainties such as the Cabibbo-Kobayashi-Maskawa matrix elements V from the $\bar{\eta}$ and $\bar{\rho}$, angles of the unitary triangle that can be neglected.

With the amplitudes calculated in Sec. III, the decay width is determined as

$$\Gamma = \frac{[(1 - (r_2 + r_3)^2)(1 - (r_2 - r_3)^2)]^{1/2}}{16\pi m_B} \sum_i |A_i|^2. \quad (50)$$

The branching ratio is got through $\mathcal{BR} = \Gamma \cdot \tau_{B_s^0}$. In Refs. [48,49], we can learn about direct CP violations, A_{CP}^{dir} is defined by

$$A_{CP}^{dir} = \frac{|\bar{A}_{\bar{f}}|^2 - |A_f|^2}{|\bar{A}_{\bar{f}}|^2 + |A_f|^2}. \quad (51)$$

Here the two amplitudes are defined as follows

$$\begin{aligned} A_f &= \langle f|\mathcal{H}|B\rangle, \\ \bar{A}_{\bar{f}} &= \langle \bar{f}|\mathcal{H}|\bar{B}\rangle, \end{aligned} \quad (52)$$

where the $\bar{B}$ meson has a b quark and $\bar{f}$ is the CP conjugate state of f. The results of the polarization fractions f_i, which are defined as

$$f_{0,\parallel,\perp} = \frac{|A_i|^2}{\sum_i |A_i|^2}, \quad (53)$$

where $A_i(i = 0, \parallel, \perp)$ is the amplitude of the longitudinal or transverse polarization contributions. Based on the helicity amplitudes $A_i(i = 0, \parallel, \perp)$ for longitudinal, parallel, and perpendicular polarizations, the three part amplitudes are given as

TABLE III.   The CP-averaged branching ratios of the $B_s^0 \to T_1 T_2$ decay (in unit of 10^{-6}), the errors attributed to the shape parameter, decay constants, hard scale, and QCD scale.

Decay modes	B_0	$B_\parallel$	$B_\perp$	B_{total}
$B_s^0 \to a_2^0 a_2^0$	$0.28^{+0.01+0.08+0.18}_{-0.03-0.02-0.01}$	$0.03^{+0.00+0.01+0.00}_{-0.00-0.00-0.00}$	0.00	$0.31^{+0.01+0.09+0.18}_{-0.03-0.02-0.01}$
$B_s^0 \to a_2^+ a_2^-$	$0.42^{+0.01+0.04+0.32}_{-0.03-0.02-0.01}$	$0.06^{+0.01+0.02+0.00}_{-0.01-0.01-0.02}$	0.00	$0.48^{+0.02+0.06+0.32}_{-0.04-0.03-0.03}$
$B_s^0 \to K_2^{*0} \bar{K}_2^{*0}$	$2.03^{+1.74+0.91+1.45}_{-1.64-0.65-1.20}$	$0.22^{+0.17+0.08+0.10}_{-0.10-0.07-0.06}$	$0.47^{+0.33+0.20+0.24}_{-0.18-0.14-0.20}$	$2.72^{+2.24+1.18+1.79}_{-1.92-0.86-1.46}$
$B_s^0 \to K_2^{*+} K_2^{*-}$	$1.86^{+1.62+0.83+1.34}_{-1.40-0.59-1.11}$	$0.21^{+0.16+0.08+0.09}_{-0.09-0.06-0.01}$	$0.19^{+0.13+0.08+0.17}_{-0.08-0.06-0.08}$	$2.26^{+1.91+0.99+1.60}_{-1.57-0.71-1.20}$
$B_s^0 \to f_2 f_2$	$0.50^{+0.04+0.08+0.24}_{-0.05-0.04-0.01}$	$0.04^{+0.00+0.01+0.00}_{-0.00-0.00-0.00}$	0.00	$0.54^{+0.04+0.09+0.24}_{-0.05-0.04-0.01}$
$B_s^0 \to f_2 f_2'$	$1.86^{+1.13+0.76+1.68}_{-0.65-0.57-0.87}$	$0.16^{+0.14+0.07+0.17}_{-0.07-0.05-0.01}$	$0.44^{+0.31+0.08+0.42}_{-0.17-0.07-0.30}$	$2.46^{+1.58+0.91+2.27}_{-0.89-0.69-1.18}$
$B_s^0 \to f_2' f_2'$	$6.03^{+0.84+1.68+4.51}_{-2.38-1.86-3.49}$	$0.42^{+0.38+0.14+0.01}_{-0.21-0.12-0.02}$	$1.23^{+1.23+0.47+0.01}_{-0.65-0.38-0.16}$	$7.68^{+2.45+2.29+4.53}_{-3.24-2.36-3.67}$

$$A_0 = \xi m_{B_s^0}^2 A_L, \qquad A_\| = \xi \sqrt{2} m_{B_s^0}^2 A_N,$$

$$A_\perp = \xi \sqrt{2(r^2 - 1)} m_{B_s^0}^2 r_2 r_3 A_T, \qquad (54)$$

here $\xi = \sqrt{\frac{G_F^2 P_c}{(16\pi m_B^2 \Gamma)}}$, and the ratio $r = \frac{P_2 \cdot P_3}{(m_B^2 r_2 r_3)}$.

Table III displays the pertinent data. Several observations can be made: (1) For $B_s^0 \to a_2^0 a_2^0, a_2^+ a_2^-, f_2 f_2$, they are only the pure annihilation diagrams, whose branching ratios are at the order of 10^{-7}. For $B_s^0 \to f_2' f_2', f_2 f_2', K_2^{*0} \bar{K}_2^{*0}, K_2^{*+} K_2^{*-}$, they have the annihilation and emission diagrams, whose branching ratios are at the order of 10^{-6}. Under the $SU(3)$ limit, since the Bose statistics are satisfied, the meson wave function will be antisymmetric when the momenta fractions of the quark and antiquark of tensor mesons are exchanged [42,43]. Due to the commutative antisymmetry of the tensor meson wave function, the nonfactorizable emission diagrams will be more pronounced and provide a greater contribution [42,43]. Take $B_s^0 \to f_2' f_2'$ for example, if without nonfactorizable emission contributions, the branching ratio will decrease 90%, and its longitudinal polarization fraction will also reduce largely, which is different from the $B_s^0 \to f_1(1420) f_1(1420)$ in Ref. [26]. For $B_s^0 \to f_1(1420) f_1(1420)$, the annihilation diagrams could contribute a large imaginary part and play an important role in calculating the branching ratios. The reason for the difference may be that, relative to the commutative antisymmetry of the tensor meson wave function, nonfactorizable emission contributions do not get offset but enhanced.

(2) From the Ref. [2], we find that $\mathcal{BR}(B_s^0 \to \phi(K_2^{*-}(1430), \bar{K}_2^{*0}(1430)))$ and $\mathcal{BR}(B_s^0 \to \phi(K^{*-}(1430) \times \bar{K}^{*0}(1430)))$ are at the same order, but the former is a little small. The authors observed that only small effects when $K^{*0}(1430)$ is substituted by $K_2^*(1430)$. We observe the corresponding decays in Ref. [8], such as $B_s^0 \to K_0^{*\pm}(1430) K^\pm$ and $B_s^0 \to K_0^*(1430) \bar{K}^0$, the branching ratio is also at the order of 10^{-5} when vector mesons are replaced by tensor mesons. The branching ratio of $B_s^0 \to K^{*0}(1430) \bar{K}_2^{*0}(1430)$ or $B_s^0 \to K_2^{*0}(1430) \bar{K}^{*0}(1430)$ is at the order of $6 \times 10^{-6} \sim 9 \times 10^{-6}$, and the branching ratio of $B_s^0 \to K_2^{*0}(1430) \bar{K}_2^{*0}(1430)$ is at the order of 2.71×10^{-6} in this paper, which also supports the view of the authors of Ref. [2].

(3) For $B_s^0 \to VT(a_2, f_2)$, when a vector meson is emitted, the factorizable emission contribution of the penguin diagrams will offset the contribution of the tree annihilation diagrams, and the branching ratio turn to be very small. However, the contribution of the annihilation diagrams does not get offset due to the absence of factorizable emission diagrams in $B_s^0 \to TT$. Therefore, the branching ratio of $B_s^0 \to TT(a_2, f_2)$ is one or two orders of magnitude larger than that of $B_s^0 \to VT(a_2, f_2)$, making it more beneficial to experimental observation.
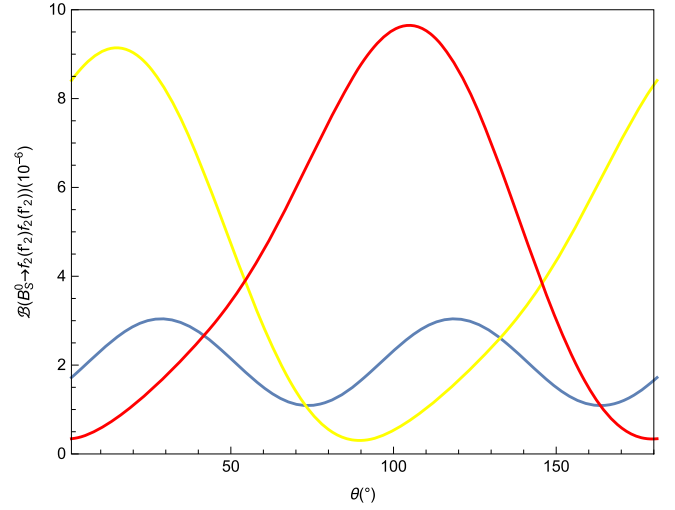

FIG. 2. The branching ratio of $B_s^0 \to f_2(f_2') f_2(f_2')$ decay on the mixing angle θ, in which the red, the yellow, and the blue solid lines correspond to the B_s^0 decays with final states $f_2(1270) f_2(1270)$, $f_2'(1525) f_2'(1525)$, and $f_2(1270) f_2'(1525)$, respectively.

(4) For $B_s^0 \to f_2(f_2') f_2(f_2')$ decays with $f_2(1270) - f_2'(1525)$ mixing, just as the $\eta - \eta'$ mixing. To see the variation clearly with the mixing angle, we show the branching ratios $\mathcal{B}$ $(B_s^0 \to f_2(f_2') f_2(f_2'))$ varying with $\theta \in [0, \pi]$ in Fig. 2. In Ref. [26], the authors plotted the related figures about the branching ratios of $B_s^0 \to f_1 f_1$ decays dependent on the free parameter θ. By comparing figures about $B_s^0 \to f_1 f_1$ and $B_s^0 \to f_2(f_2') f_2(f_2')$, we can find that when the θ is large enough, and its influence on the branching ratio is more obvious, which can be seen from the line shapes. When θ reaches a certain angle, the branching ratios of $B_s^0 \to f_2(f_2') f_2(f_2')$ and $B_s^0 \to f_1 f_1$ will vary an order of magnitude. But for $f_2(1270) - f_2'(1525)$ mixing, in the contrast to $f_1(1285) - f_1(1420)$, the mixing angle is very small. From the Refs. [24,25,50], we have known that the mixing θ is about $5.8° \sim 10°$, and the related branching ratios are close to that of $0°$. In addition, the branching ratio of the $B_s^0 \to f_2'(1525) f_2'(1525)$ decay is larger than that of the $B_s^0 \to f_2(1270) f_2(1270)$ decay by one order of magnitude, which is caused due to the reason that the former has more Feynman diagrams.

B_s^0 mesons can be produced in the $\Upsilon(5S)$ decays to $B_s^0 \bar{B}_s^0$, $B_s^0 \bar{B}_s^*$, $B_s^* \bar{B}_s^0$, or $B_s^* \bar{B}_s^*$ intermediate decay [51]. Since of the kinematic smearing from excited B_s^* production and contamination from $B^{+/0}$ decays, measurements are not as easy as at the $\Upsilon(4S)$. Although full B_s^0 reconstruction would mitigate $B^{+/0}$ background, such a technique will only be possible with Belle II [52]. The number of B_s^0 mesons in a dataset can be calculated as $N_{B_s^0} = 2 \times \sigma_{b\bar{b}}^{\Upsilon(5S)} \times f_s \times \mathcal{L}$. The parameter f_s is a key component to calculate the total B_s^0 yield in the sample. $\mathcal{L}$ is the integrated luminosity of the

TABLE IV. Presents the polarization fraction of the decay. The accompanying errors arise from considerations encompassing the shape parameter, decay constants, hard scale, and QCD scale.

Decay modes	f_0	$f_\parallel$	$f_\perp$
$B_s^0 \to a_2^0 a_2^0$	$90.92^{+0.11+0.15+3.58}_{-0.45-0.05-0.53}\%$	$8.88^{+0.46+0.06+0.56}_{-0.12-0.14-3.56}\%$	0.19%
$B_s^0 \to a_2^+ a_2^-$	$88.24^{+0.29+0.65+6.83}_{-0.83-1.81-0.52}\%$	$11.66^{+0.84+1.79+0.54}_{-0.30-0.65-6.82}\%$	0.09%
$B_s^0 \to K_2^{*0}\bar{K}_2^{*0}$	$75.02^{+1.22+0.43+2.40}_{-25.37-0.55-14.29}\%$	$8.08^{+7.58+0.14+12.27}_{-0.16-0.30-1.05}\%$	$16.89^{+18.01+0.42+2.03}_{-1.05-0.13-1.38}\%$
$B_s^0 \to K_2^{*+} K_2^{*-}$	$82.50^{+1.01+0.43+0.46}_{-15.80-0.38-11.02}\%$	$9.16^{+7.70+0.16+9.44}_{-0.41-0.35-1.46}\%$	$8.34^{+8.10+0.22+0.99}_{-0.60-0.09-1.64}\%$
$B_s^0 \to f_2 f_2$	$93.7^{+0.01+0.77+2.35}_{-0.07-0.74-0.38}\%$	$6.78^{+0.08+0.73+0.40}_{-0.02-0.75-2.33}\%$	0.14%
$B_s^0 \to f_2 f_2'$	$75.78^{+1.44+2.22+2.70}_{-1.61-2.78-7.92}\%$	$6.32^{+0.99+0.18+15.90}_{-0.88-0.30-3.18}\%$	$17.91^{+0.60+3.07+0.47}_{-0.57-2.47-7.99}\%$
$B_s^0 \to f_2' f_2'$	$78.56^{+3.78+0.31+7.94}_{-10.88-1.28-15.12}\%$	$5.44^{+2.45+0.19+4.42}_{-0.77-0.01-1.96}\%$	$16.99^{+8.43+1.09+10.69}_{-3.02-0.06-5.99}\%$

data and $\sigma_{b\bar{b}}^{\Upsilon(5S)}$ is the cross section of the process $e^+ e^- \to b\bar{b}$ [51,53]. By using the values from the Refs. [54,55], the number of B_s^0 mesons is estimated to be $\sim 5.9 \times 10^8$ in the dataset of $\mathcal{L} = 5$ ab^{-1} taken at $\Upsilon(5S)$ in Belle II [51], which indicates that a 5 ab$^{-1}\Upsilon(5S)$ sample contains approximately 300 million $B_s^0 \bar{B}_s^0$ pairs. The branching ratios of our calculation for $B_s^0 \to TT$ are at the order of 10^{-6} and 10^{-7}. Therefore, the decays of $B_s^0 \to TT$ will hopefully be observed by the Belle II experiments in the near future.

Moving on to Table IV, we delve into predictions pertaining to the polarization fraction of mesons. The pQCD approach has effectively elucidated the theoretical underpinnings of pure annihilation diagrams about $B_s^0 \to \pi^+\pi^-$ and $B^0 \to D_S^- K^+$ theoretically, and corresponding numerical results has been confirmed by experiments. Based on this success, it is plausible to assert that the pQCD approach holds substantial predictive power for processes primarily governed by annihilation diagrams [4,56–58]. In line with prior research [3,59], it has been ascertained that the contributions to these processes are chiefly orchestrated by longitudinal polarization in the case of pure annihilation of two-body decays. The fractions pertaining to these decays have been observed to approach nearly 100%. This trend corroborates our predictions of

$B_s^0 \to f_2 f_2$, $B_s^0 \to a_2^0 a_2^0$, and $B_s^0 \to a_2^+ a_2^-$. Notably, the longitudinal polarizations of these three decays approximate 90%, underscoring the indispensability of accounting for transverse polarization, which can yield noteworthy contributions in pure annihilation decays. To illustrate this point, we take $B_s^0 \to a_2^0 a_2^0$ and $B_s^0 \to f_2 f_2$ as an example, from Table VI reveals that the contribution of longitudinal polarization surpasses that of transverse polarization, rendering the former the predominant factor.

Across all the decays calculated in this study, longitudinal polarization predominantly steers the main decay modes. Through a factorial power estimation, it is evident that longitudinal polarization will play a leading role in the B meson decay [60,61]. For $B_s^0 \to TT$, in the longitudinal polarization part, the contribution of nonfactorizable emission diagrams is substantial, and the extent of cancellation with annihilation diagrams is notably feeble. Conversely, in the transverse polarization segment, nonfactorizable emission diagrams contribute minimally, and this contribution effectively counterbalances the annihilation contribution. Consequently, longitudinal polarization prevails, and the transverse polarization fraction is about 10%–30%.

Direct CP asymmetries of $B_s^0 \to TT$ decays are listed in Table V. The magnitude of the direct CP violation is proportional to the ratio of the penguin and tree

TABLE V. The CP-violating asymmetries of the $B_s^0 \to T_1 T_2$ decay, the errors come from the shape parameter, decay constants, hard scale, and QCD scale.

Decay modes	$\mathcal{A}_{CP}^{dir}$	$\mathcal{A}_{CP}^{dir}(0)$	$\mathcal{A}_{CP}^{dir}(\parallel)$	$\mathcal{A}_{CP}^{dir}(\perp)$
$B_s^0 \to a_2^0 a_2^0$	$(3.30^{+3.34+11.88+13.19}_{-3.75-1.77-38.50})\%$	$(3.39^{+4.05+15.04+17.03}_{-4.62-2.19-44.62})\%$	$(2.21^{+0.61+0.13+0.31}_{-0.62-0.15-0.24})\%$	$(13.80^{+0.88+1.23+1.10}_{-0.90-1.23-1.58})\%$
$B_s^0 \to f_2 f_2$	$(-6.12^{+3.06+5.93+9.96}_{-3.00-3.45-33.23})\%$	$(-6.73^{+3.25+6.34+10.71}_{-4.64-2.35-34.63})\%$	$(1.80^{+0.48+0.14+0.25}_{-0.46-0.15-0.31})\%$	$(9.14^{+0.64+0.89+1.87}_{-0.03-0.90-1.59})\%$
$B_s^0 \to K_2^{*0}\bar{K}_2^{*0}$	0.00%	$\cdots$	$\cdots$	$\cdots$
$B_s^0 \to f_2 f_2'$	$(1.04^{+0.19+1.81+8.43}_{-0.68-0.35-4.58})\%$	$(1.04^{+0.31+0.25+3.38}_{-0.55-0.29-7.51})\%$	$(-71.35^{+2.18+0.10+19.17}_{-1.68-0.11-7.38})\%$	$(26.72^{+6.84+2.83+18.02}_{-6.20-0.57-4.90})\%$
$B_s^0 \to f_2' f_2'$	0.00%	$\cdots$	$\cdots$	$\cdots$
$B_s^0 \to a_2^+ a_2^-$	$(2.09^{+2.58+11.87+10.92}_{-3.03-1.46-22.78})\%$	$(2.21^{+2.58+11.87+10.92}_{-3.03-1.46-22.78})\%$	$(1.06^{+0.30+0.07+61.22}_{-0.29-0.07-0.12})\%$	$(17.54^{+0.98+1.84+0.81}_{-1.02-1.79-1.84})\%$
$B_s^0 \to K_2^{*+} K_2^{*-}$	$(2.61^{+3.94+0.77+6.18}_{-36.51-0.70-5.13})\%$	$(3.57^{+3.74+0.99+6.66}_{-53.07-0.99-9.60})\%$	$(-2.44^{+0.05+0.12+3.51}_{-0.33-0.43-3.87})\%$	$(-0.91^{+6.62+0.70+2.48}_{-0.84-0.28-4.33})\%$

TABLE VI. Decay amplitudes (in unit of 10^{-3} GeV^3) of the $B_s^0 \to T_1 T_2$ modes with three polarizations in the pQCD approach, where only the central values are quoted for clarification.

Components classification	$B_s^0 \to a_2^0 a_2^0$ Tree diagrams	$B_s^0 \to a_2^0 a_2^0$ Penguin diagrams	$B_s^0 \to f_2 f_2$ Tree diagrams	$B_s^0 \to f_2 f_2$ Penguin diagrams
A_L	$0.157 - 0.130i$	$-0.082 - 0.224i$	$-0.290 - 0.304i$	$-0.353 - 0.615i$
A_N	$-0.014 + 0.025i$	$0.104 + 0.135i$	$-0.015 + 0.030i$	$0.130 + 0.148i$
A_T	$0.010 + 0.017i$	$-7.887 \times 10^{-3} + 3.704 \times 10^{-3}i$	$0.011 + 0.020i$	$-9.728 \times 10^{-3} + 3.298 \times 10^{-3}i$

contributions [50]. For the $B_s^0 \to VV$ and $B_s^0 \to VT$, when penguin contributions and tree contributions stay at the same level, the direct CP violation appears. Since the decays presented in this paper are dominated by the penguin contributions, so the direct CP violation is very small. However, we can find that the direct CP violations of some special channels in the transverse polarization are sizable, and the tree contributions become comparable, which brings relatively large direct CP violation.

For pure annihilation-type decay, the CP-violating asymmetry is small, which has been pointed out in previous predictions of two-body decays [3,59]. From Table V, the CP-violating asymmetries about $B_s^0 \to a_2^0 a_2^0, f_2 f_2$, and $a_2^+ a_2^-$, which also suggest that the CP-violating asymmetry of pure annihilation decay is very small. For $B_s^0 \to K_2^{*0}(1430)\bar{K}_2^{*0}(1430)$, $f_2'(1525)f_2'(1525)$ (without considering the mixing angle), in the standard model, there is no contribution of the tree diagrams operator, so the direct CP violation is zero.

V. SUMMARY

In this study, we predicted the relevant parameters of decays $B_s^0 \to TT$ in the pQCD approach, where the tensor mesons are $a_2(1320)$, $f_2(1270)$, $K_2^*(1430)$, and $f_2'(1525)$. We calculate the branching ratios, the polarization fractions, and the direct CP violations of these decays. Our calculation results suggest that (1) the production of tensor mesons via either vector or tensor currents is prohibited, highlighting the significance of nonfactorizable emission and annihilation contributions. Notably, the nonfactorizable emission

diagram exhibits an augmented contribution owing to the antisymmetry inherent in the tensor meson wave function. (2) For decays characterized exclusively by annihilation processes, the branching ratio is situated at an order of 10^{-7}. And for $f_2'(1525)$, $K_2^*(1430)$, they have a sizable branching ratio with the order of 10^{-6}, which would be easy to be verified experimentally. (3) Regarding polarization fractions, the preponderance of the decay processes investigated in this paper predominantly manifests longitudinal contributions, particularly in the case of pure annihilation decay, where it can reach around 90%. (4) The direct CP violations associated with these decays are of nominal magnitude. The interference between penguin and tree contributions will bring the direct violations, and the two components assessed in this paper are not comparable. Consequently, the direct CP violations in the majority of channels remain negligible, with only select channels exhibiting relatively pronounced direct CP violation appears. In conclusion, we anticipate that our results can be scrutinized through forthcoming experiments at LHC-b and Belle II. Furthermore, we hope that these findings contribute positively to our understanding of the QCD behavior of tensor mesons.

ACKNOWLEDGMENTS

APPENDIX: FORMULAS FOR THE CALCULATION USED IN THE TEXT

In this section, we list the helicity amplitudes for every considered two-body decays of B meson.

$$
\begin{aligned}
A_h(B_s^0 \to a_2^0(1320)a_2^0(1320)) = G_F \Bigg(& V_{ub}^* V_{us} \left[\left(C_1 + \frac{1}{3} C_2 \right) F_a^{LL,h} + C_2 M_a^{LL,h} \right] \\
& - V_{tb}^* V_{ts} \left[\left(2C_3 + \frac{2}{3} C_4 + 2C_5 + \frac{2}{3} C_6 + \frac{1}{2} C_7 + \frac{1}{6} C_8 + \frac{1}{2} C_9 + \frac{1}{6} C_{10} \right) F_a^{LL,h} \right. \\
& \left. + \left(2C_4 + \frac{1}{2} C_{10} \right) M_a^{LL,h} + \left(2C_6 + \frac{1}{2} C_8 \right) M_a^{SP,h} \right] \Bigg)
\end{aligned}
\tag{A1}
$$

and $B_s^0 \to f_2(1270)f_2(1270)$ decay has the same amplitude as $B_s^0 \to a_2^0(1320)a_2^0(1320)$ decays.

$$
\begin{aligned}
A_h(B_s^0 \to K_2^*(1430)\bar{K}_2^*(1430)) = &-G_F\left(V_{tb}^*V_{ts}\left[\left(\frac{7}{3}C_3 + \frac{5}{3}C_4 - \frac{7}{6}C_9 - \frac{5}{6}C_{10}\right)F_a^{LL,h}\right.\right. \\
&+ 2\left(C_5 + \frac{1}{3}C_6 - \frac{1}{2}C_7 - \frac{1}{6}C_8\right)F_a^{LR,h} + \left(-\frac{1}{2}C_8 - \frac{1}{6}C_7 + C_6 + \frac{1}{3}C_5\right)F_a^{SP,h} \\
&+ \left(C_3 - \frac{1}{2}C_9\right)M_e^{LL,h} + \left(C_5 - \frac{1}{2}C_7\right)M_e^{LR,h} + \left(C_3 + 2C_4 - \frac{1}{2}C_9 - C_{10}\right)M_a^{LL,h} \\
&+ \left.\left.(2C_6 - C_8)M_a^{SP,h} + \left(C_5 - \frac{1}{2}C_7\right)M_a^{LR,h}\right]\right),
\end{aligned}
\tag{A2}
$$

$$
\begin{aligned}
A_h(B_s^0 \to f_2'(1525)f_2'(1525)) = &-G_F V_{tb}^*V_{ts}\left[\left(\frac{4}{3}C_3 + \frac{4}{3}C_4 - \frac{2}{3}C_9 - \frac{2}{3}C_{10}\right)F_a^{LL,h}\right. \\
&+ \left(C_5 + \frac{1}{3}C_6 - \frac{1}{2}C_7 - \frac{1}{6}C_8\right)F_a^{LR,h} + \left(C_6 + \frac{1}{3}C_5 - \frac{1}{2}C_8 - \frac{1}{6}C_7\right)F_a^{SP,h} \\
&+ \left(C_3 + C_4 - \frac{1}{2}C_9 - \frac{1}{2}C_{10}\right)M_e^{LL,h} + \left(C_5 - \frac{1}{2}C_7\right)M_e^{LR,h} \\
&+ \left(C_3 + C_4 - \frac{1}{2}C_9 - \frac{1}{2}C_{10}\right)M_a^{LL,h} + \left(C_6 - \frac{1}{2}C_8\right)M_a^{SP,h} \\
&+ \left.\left(C_5 - \frac{1}{2}C_7\right)M_a^{LR,h} + \left(C_6 - \frac{1}{2}C_8\right)M_e^{SP,h}\right],
\end{aligned}
\tag{A3}
$$

$$
\begin{aligned}
A_h(B_s^0 \to f_2(1270)f_2'(1525)) = &\frac{G_F}{2}\left(V_{ub}^*V_{us}[C_2 M_e^{LL,h}] - V_{tb}^*V_{ts}\left[\left(2C_4 + \frac{1}{2}C_{10}\right)M_e^{LL,h}\right.\right. \\
&+ \left.\left.\left(\frac{1}{2}C_8 + 2C_6\right)M_e^{SP,h}\right]\right),
\end{aligned}
\tag{A4}
$$

$$
\begin{aligned}
A_h(B_s^0 \to a_2^+(1320)a_2^-(1320)) = &\frac{G_F}{\sqrt{2}}\left(V_{ub}^*V_{us}\left[\left(C_1 + \frac{1}{3}C_2\right)F_a^{LL,h} + C_2 M_a^{LL,h}\right]\right. \\
&- 2V_{tb}^*V_{ts}\left[\left(2C_3 + \frac{2}{3}C_4 + 2C_5 + \frac{2}{3}C_6 + \frac{1}{2}C_7 + \frac{1}{6}C_8 + \frac{1}{2}C_9 + \frac{1}{6}C_{10}\right)F_a^{LL,h}\right. \\
&+ \left.\left.\left(2C_4 + \frac{1}{2}C_{10}\right)M_a^{LL,h} + \left(2C_6 + \frac{1}{2}C_8\right)M_a^{SP,h}\right]\right),
\end{aligned}
\tag{A5}
$$

$$
\begin{aligned}
A_h(B_s^0 \to K_2^{*+}(1430)\bar{K}_2^{*-}(1430)) = &\frac{G_F}{\sqrt{2}}\left(V_{ub}^*V_{us}\left[\left(C_1 + \frac{1}{3}C_2\right)F_a^{LL,h} + C_2 M_a^{LL,h} + C_1 M_e^{LL,h}\right]\right. \\
&- V_{tb}^*V_{ts}\left[\left(\frac{7}{3}C_3 + \frac{5}{3}C_4 + \frac{1}{3}C_9 - \frac{1}{3}C_{10}\right)F_a^{LL,h} + \left(2C_5 + \frac{2}{3}C_6 + \frac{1}{2}C_7 + \frac{1}{6}C_8\right)F_a^{LR,h}\right. \\
&+ \left(-\frac{1}{2}C_8 - \frac{1}{6}C_7 + C_6 + \frac{1}{3}C_5\right)F_a^{SP,h} + (C_3 + C_9)M_e^{LL,h} \\
&+ (C_5 + C_7)M_e^{LR,h} + \left(C_3 + 2C_4 + \frac{1}{2}C_9 - C_{10}\right)M_a^{LL,h} \\
&+ \left.\left.\left(2C_6 + \frac{1}{2}C_8\right)M_a^{SP,h} + \left(C_5 - \frac{1}{2}C_7\right)M_a^{LR,h}\right]\right).
\end{aligned}
\tag{A6}
$$

Based on the mixing scheme, the helicity amplitudes of $B_s^0 \to f_n f_n (f_s f_s)$ and $B_s^0 \to f_n f_s$ decays are given by [26]

$$A_h(B_s^0 \to f_2(1270)f_2'(1525)) = \sin(2\theta)[A_h(B_s^0 \to f_n f_n) - A_h(B_s^0 \to f_s f_s)] + \cos(2\theta)A_h(B_s^0 \to f_n f_s), \quad (A7)$$

$$\sqrt{2}A_h(B_s^0 \to (f_2(1270)f_2(1270)) = 2\cos^2\theta A_h(B_s^0 \to f_n f_n) - \sin(2\theta)A_h(B_s^0 \to f_n f_s) + 2\sin^2\theta A_h(B_s^0 \to f_s f_s), \quad (A8)$$

$$\sqrt{2}A_h(B_s^0 \to (f_2'(1525)f_2'(1525)) = 2\sin^2\theta A_h(B_s^0 \to f_n f_n) + \sin(2\theta)A_h(B_s^0 \to f_n f_s) + 2\cos^2\theta A_h(B_s^0 \to f_s f_s). \quad (A9)$$

In this part, we summarize the functions that appear in the previous sections. For the factorizable annihilation diagrams that the first two diagrams in the Fig. 1, whose hard scales t_i can be written by

$$t_e = \text{Max}\left\{\alpha_1 M_{B_s^0}, \beta M_{B_s^0}, \frac{1}{b_2}, \frac{1}{b_3}\right\},$$

$$t_f = \text{Max}\left\{\alpha_2 M_{B_s^0}, \beta M_{B_s^0}, \frac{1}{b_2}, \frac{1}{b_3}\right\},$$

$$h_{af}(\alpha_i, \beta, b_2, b_3) = \left(\frac{i\pi}{2}\right)^2 H_0^{(1)}(\beta M_{B_s^0} b_2) \times [\theta(b_2 - b_3)H_0^{(1)}(\alpha_i M_{B_s^0} b_2)J_0(\alpha_i M_{B_s^0} b_3)$$

$$+ \theta(b_3 - b_2)H_0^{(1)}(\alpha_i M_{B_s^0} b_3)J_0(\alpha_i M_{B_s^0} b_2)]S_t(x_3), \quad (A10)$$

with

$$\alpha_1 = \sqrt{1 - (1 - r_2^2)x_3},$$

$$\alpha_2 = \sqrt{[(1 - r_3^2)x_2 + r_3^2](1 - r_2^2)},$$

$$\beta = \sqrt{[(1 - r_2^2)(1 - x_3)][r_3^2 + x_2(1 - r_3^2)]}. \quad (A11)$$

The parametrized expression of the threshold resummation function $S_t(x)$ is [34]

$$S_t(x) = [x(1 - x)]^c \frac{2^{1+2c}\Gamma\left(\frac{3}{2} + c\right)}{\sqrt{\pi}\Gamma(1 + c)}, \quad (A12)$$

where $c = 0.04$. The evolution factors $E_{af}(t)$ in the matrix elements are given by

$$E_{af}(t) = \alpha_s(t)\exp[-S_2(t) - S_3(t)]. \quad (A13)$$

The Sudakov exponents can be written as

$$S_B(t) = s\left(x_1 \frac{M_{B_s^0}}{\sqrt{2}}, b_1\right) + \frac{5}{3}\int_{1/b_1}^t d\bar{\mu}\frac{\gamma_q(\alpha_s(\bar{\mu}))}{\bar{\mu}},$$

$$S_i(t) = s\left(x_i \frac{M_{B_s^0}}{\sqrt{2}}, b_i\right) + s\left((1 - x_i)\frac{M_{B_s^0}}{\sqrt{2}}, b_i\right)$$

$$+ 2\int_{1/b}^t d\bar{\mu}\frac{\gamma_q(\alpha_s(\bar{\mu}))}{\bar{\mu}}, \quad (A14)$$

where the Sudakov factors $s(Q, b)$ are derived from the double logarithmic summation. Its specific expression can be found in the Ref. [62]. For the nonfactorizable contribution, due to the small numerical effect, we drop the threshold resummation function [28]. For the nonfactorizable annihilation diagrams, the scales and the hard functions are [63]

$$t_g = \text{Max}\left\{\alpha M_{B_s^0}, \sqrt{|\beta_1|}M_{B_s^0}, \frac{1}{b_1}, \frac{1}{b_2}\right\},$$

$$t_h = \text{Max}\left\{\alpha M_{B_s^0}, \sqrt{|\beta_2|}M_{B_s^0}, \frac{1}{b_1}, \frac{1}{b_2}\right\},$$

$$E_{anf}(t) = \alpha_s(t)\exp[-S_B(t) - S_2(t) - S_3(t)]|_{b_2=b_3},$$

$$h_{anf}(\alpha, \beta_i, b_1, b_2) = \frac{i\pi}{2}[\theta(b_1 - b_2)H_0^{(1)}(\alpha M_{B_s^0}b_1)J_0(\alpha M_{B_s^0}b_2) + \theta(b_2 - b_1)H_0^{(1)}(\alpha M_{B_s^0}b_2)J_0(\alpha M_{B_s^0}b_1)]$$

$$\times \begin{cases} \frac{i\pi}{2}H_0^{(1)}(M_{B_s^0}b_1\sqrt{|\beta_i|}), & \beta_i < 0 \\ K_0(M_{B_s^0}b_1\sqrt{\beta_i}), & \beta_i > 0 \end{cases}, \tag{A15}$$

with $i = 1, 2$

$$\alpha = \sqrt{(1 - x_3)(1 - r_2^2)[r_3^2 + x_2(1 - r_3^2)]},$$

$$\beta_1 = 1 - [(1 - r_3^2)(1 - x_2) - x_1][r_2^2 + x_3(1 - r_2^2)],$$

$$\beta_2 = (1 - r_2^2)(1 - x_3)[x_1 - x_2(1 - r_3^2) - r_3^2]. \tag{A16}$$

For the nonfactorizable emission diagrams, the rest functions are follows

$$t_c = \text{Max}\left\{M_{B_s^0}\sqrt{(1 - r_2^2)x_1x_3}, M_{B_s^0}\sqrt{|[(1 - r_3^2)(x_2 - 1) + x_1][r_2^2 + x_3(1 - r_2^2)]|}, \frac{1}{b_1}, \frac{1}{b_2}\right\},$$

$$t_d = \text{Max}\left\{M_{B_s^0}\sqrt{(1 - r_2^2)x_1x_3}, M_{B_s^0}\sqrt{|[(r_3^2 - 1)x_2 + x_1]x_3(1 - r_2^2)|}, \frac{1}{b_1}, \frac{1}{b_2}\right\}. \tag{A17}$$

The function h_{enf} can be determined by

$$h_{enf}(\alpha, \beta_i, b_1, b_2) = [\theta(b_2 - b_1)I_0(\alpha b_1)K_0(\alpha b_2) + \theta(b_1 - b_2)I_0(\alpha b_2)K_0(\alpha b_1)]$$

$$\times \begin{cases} \frac{i\pi}{2}H_0^{(1)}(M_{B_s^0}b_2\sqrt{|\beta_i^2|}), & \beta_i^2 < 0 \\ K_0(M_{B_s^0}b_2\beta_i), & \beta_i^2 > 0 \end{cases}, \tag{A18}$$

with $i = 1, 2$

$$E_{enf}(t) = \alpha_s(t)\exp[-S_B(t) - S_2(t) - S_3(t)]|_{b_1=b_3},$$

$$\alpha = M_{B_s^0}\sqrt{(1 - r_2^2)x_1x_3},$$

$$\beta_1^2 = [(1 - r_3^2)(x_2 - 1) + x_1][r_2^2 + x_3(1 - r_2^2)],$$

$$\beta_2^2 = [(r_3^2 - 1)x_2 + x_1]x_3(1 - r_2^2). \tag{A19}$$

[1] X. Liu, R. H. Li, Z. T. Zou, and Z. J. Xiao, Nonleptonic charmless decays of $B_c \to TP, TV$ in the perturbative QCD approach, Phys. Rev. D **96**, 013005 (2017).

[2] C. S. Kim, R. H. Li, F. Simanjuntak, and Z. T. Zou, Charmless $B_{u,d,s} \to VT$ decays in perturbative QCD approach, Phys. Rev. D **88**, 014031 (2013).

[3] Z. T. Zou, A. Ali, C. D. Lu, X. Liu, and Y. Li, Improved estimates of the $B_{(s)} \to VV$ decays in perturbative QCD approach, Phys. Rev. D **91**, 054033 (2015).

[4] A. Ali, G. Kramer, Y. Li, C. D. Lu, Y. L. Shen, W. Wang, and Y. M. Wang, Charmless non-leptonic B_s decays to PP, PV and VV final states in the pQCD approach, Phys. Rev. D **76**, 074018 (2007).

[5] J. H. Munoz, A. A. Rojas, and G. Lopez Castro, Cabibbo suppressed nonleptonic B decays and D decays involving tensor mesons, Phys. Rev. D **59**, 077504 (1999).

[6] B. Aubert *et al.* (BABAR Collaboration), Observation and polarization measurements of $B^\pm \to \phi K_1^\pm$ and $B^\pm \to \phi K_2^{*\pm}$, Phys. Rev. D **101**, 161801 (2008).

[7] B. Aubert *et al.* (BABAR Collaboration), Time-dependent and time-integrated angular analysis of $B \to \phi K_s^0 \pi^0$ and $\phi K^\pm \pi^\pm$, Phys. Rev. D **78**, 092008 (2008).

[8] R. L. Workman *et al.* (Particle Data Group), Particle data group webpage, http://pdg.lbl.gov/.

[9] W. Wang, B to tensor meson form factors in the perturbative QCD approach, Phys. Rev. D **83**, 014008 (2011).

[10] K. Nakamura *et al.* (Particle Data Group), Review of particle physics, J. Phys. G **37**, 075021 (2010).

[11] D. C. Yan, X. Liu, and Z. J. Xiao, Anatomy of $B_s \to VV$ decays and effects of next-to-leading order contributions in the perturbative QCD factorization approach, Nucl. Phys. **B935**, 17 (2018).

[12] Y. Li, D. C. Yan, Z. Rui, and Z. J. Xiao, Study of $B_{(s)} \to (\pi\pi)(K\pi)$ decays in the perturbative QCD approach, Eur. Phys. J. C **81**, 806 (2021).

[13] Z. Rui, Y. Li, and H. n. Li, Four-body decays $B_{(s)} \to (K\pi)_{S/P}(K\pi)_{S/P}$ in the perturbative QCD approach, J. High Energy Phys. 05 (2021) 082.

[14] H. Q. Liang and X. Q. Yu, Study of the four-body decays $B_s^0 \to \pi\pi\pi\pi$ in the perturbative QCD approach, Phys. Rev. D **105**, 096018 (2022).

[15] H. Yang and X. Q. Yu, Investigating Bs three-body decays of scalar mesons in perturbative QCD approach, Phys. Rev. D **107**, 013001 (2023).

[16] W. Liu and X. Q. Yu, Contributions of S-, P-, and D-wave resonances to the quasi-two-body decays $B_s^0 \to \psi(3686, 3770)K\pi$ in the perturbative QCD approach, Eur. Phys. J. C **82**, 441 (2022).

[17] Z. R. Liang and X. Q. Yu, Perturbative QCD predictions for the decay $B_s^0 \to SS(a_0(980), f_0(980), f_0(500))$, Phys. Rev. D **102**, 116007 (2020).

[18] Z. T. Zou, X. Yu, and C. D. Lu, Nonleptonic two-body charmless B decays involving a tensor meson in the perturbative QCD approach, Phys. Rev. D **86**, 094015 (2012).

[19] H. W. Huang, C. D. Lu, T. Morii, Y. L. Shen, G. Song, and Jin-Zhu, Study of $B_s^0 \to K^*\rho, K^*\omega$ decays with polarization

[20] H. n. Li and S. Mishima, Implication of the $B \to \rho\rho$ data on the $B \to \pi\pi$ puzzle, Phys. Rev. D **73**, 114014 (2006).

[21] T. Feldmann, P. Kroll, and B. Stech, Mixing and decay constants of pseudoscalar mesons, Phys. Rev. D **58**, 114006 (1998).

[22] Z. j. Xiao, D. q. Guo, and X. f. Chen, Branching ratio and CP asymmetry of $B^0 \to \eta^{(\prime)}\eta^{(\prime)}$ decays in the perturbative QCD approach, Phys. Rev. D **75**, 014018 (2007).

[23] R. Escribano and J. M. Frere, Study of the $\eta - \eta'$ system in the two mixing angle scheme, J. High Energy Phys. 06 (2005) 029.

[24] H. Y. Cheng and R. Shrock, Some results on vector and tensor meson mixing in a generalized QCD-like theory, Phys. Rev. D **84**, 094008 (2011).

[25] D. M. Li, H. Yu, and Q. X. Shen, Properties of the tensor mesons $f_2(1270)$ and $f_2'(1525)$, J. Phys. G **27**, 807 (2001).

[26] Z. Jiang, D. H. Yao, Z. T. Zou, X. Liu, Y. Li, and Z. J. Xiao, $B_{d,s}^0 \to f_1 f_1$ decays with $f_1(1285) - f_1(1420)$ mixing in the perturbative QCD approach, Phys. Rev. D **102**, 116015 (2020).

[27] K. C. Yang, Light-cone distribution amplitudes of axial-vector mesons, Nucl. Phys. **B776**, 187 (2007).

[28] H. n. Li and K. Ukai, Threshold resummation for non-leptonic B meson decays, Phys. Lett. B **555**, 197 (2003).

[29] A. J. Buras, Weak Hamiltonian, CP violation and rare decays, arXiv:hep-ph/9806471.

[30] G. Buchalla, A. J. Buras, and M. E. Lautenbacher, Weak decays beyond leading logarithms, Rev. Mod. Phys. **68**, 1125 (1996).

[31] X. Liu, Z. J. Xiao, and Z. T. Zou, Nonleptonic decays of $B \to (f_1(1285), f_1(1420))V$ in the perturbative QCD approach, Phys. Rev. D **94**, 113005 (2016).

[32] X. Liu and Z. J. Xiao, $B \to a_1(1260)a_1(1260)$ and $b_1(1235)b_1(1235)$ decays in the perturbative QCD approach, Phys. Rev. D **86**, 074016 (2012).

[33] Y. Li and C. D. Lu, Branching ratio and polarization of $B \to \rho(\omega)\rho(\omega)$ decays in perturbative QCD approach, Phys. Rev. D **73**, 014024 (2006).

[34] H. n. Li, Threshold resummation for exclusive B meson decays, Phys. Rev. D **66**, 094010 (2002).

[35] H. n. Li and B. Tseng, Nonfactorizable soft gluons in nonleptonic heavy meson decays, Phys. Rev. D **57**, 443 (1998).

[36] Y. L. Shen and Y. M. Wang, Rapidity resummation for B-meson wave functions, EPJ Web Conf. **80**, 00047 (2014).

[37] Y. Y. Keum, H. n. Li, and A. I. Sanda, Fat penguins and imaginary penguins in perturbative QCD, Phys. Lett. B **504**, 6 (2001).

[38] M. Beneke and T. Feldmann, Symmetry breaking corrections to heavy to light B meson form-factors at large recoil, Nucl. Phys. **B592**, 3 (2001).

[39] C. D. Lu, K. Ukai, and M. Z. Yang, Branching ratio and CP violation of $B \to \pi\pi$ decays in perturbative QCD approach, Phys. Rev. D **63**, 074009 (2001).

[40] T. Kurimoto, H. n. Li, and A. I. Sanda, Leading power contributions to $B \to \pi, \rho$ transition form-factors, Phys. Rev. D **65,** 014007 (2002).

[41] H. n. Li, QCD aspects of exclusive B meson decays, Prog. Part. Nucl. Phys. **51,** 85 (2003).

[42] H. Y. Cheng, Y. Koike, and K. C. Yang, Two-parton light-cone distribution amplitudes of tensor mesons, Phys. Rev. D **82,** 054019 (2010).

[43] H. Y. Cheng and K. C. Yang, Charmless hadronic B decays into a tensor meson, Phys. Rev. D **83,** 034001 (2011).

[44] T. M. Aliev and M. A. Shifman, Old tensor mesons in QCD sum rules, Phys. Lett. **112B,** 401 (1982).

[45] T. M. Aliev and M. A. Shifman, QCD sum rules and tensor mesons. (In Russian), Sov. J. Nucl. Phys. **36,** 891 (1982).

[46] T. M. Aliev, K. Azizi, and V. Bashiry, On the mass and decay constant of $K_2^*(1430)$ tensor meson, J. Phys. G **37,** 025001 (2010).

[47] Particle Date Group, Review of particle physics, Prog. Theor. Exp. Phys. **2020,** 083C01 (2020).

[48] I. I. Bigi and A. I. Sanda, *CP* violation, Cambridge Monogr. Part. Phys., Nucl. Phys., Cosmol. **9,** 1 (2009).

[49] G. C. Branco, L. Lavoura, and J. P. Silva, *CP Violation* (Oxford University Press, Oxford, 1999).

[50] C. Amsler *et al.* (Particle Data Group), Review of particle physics, Phys. Lett. B **667,** 1 (2008).

[51] T. Aushev, W. Bartel, A. Bondar, J. Brodzicka, T. E. Browder, P. Chang, Y. Chao, K. F. Chen, J. Dalseno, A. Drutskoy *et al.*, Physics at super B factory, arXiv:1002.5012.

[52] P. Urquijo, Semileptonic B_s decays at Belle, *BABAR*, and D0, arXiv:1305.1234.

[53] C. Oswald and T. K. Pedlar, Results in B_s physics and bottomonium spectroscopy using the Belle $\Upsilon(5S)$ data, Mod. Phys. Lett. A **28,** 1330036 (2013).

[54] G. S. Huang *et al.* (CLEO Collaboration), Measurement of $B(\Upsilon(5S)) \to B_s^* \bar{B}_s^*$ using ϕ mesons, Phys. Rev. D **75,** 012002 (2007).

[55] A. Drutskoy *et al.* (Belle Collaboration), Measurement of inclusive D_s, D^0 and J/ψ rates and determination of the $B_s^{(*)} \bar{B}_s^{(*)}$ production fraction in $b\bar{b}$ events at the $\Upsilon(5S)$ resonance, Phys. Rev. Lett. **98,** 052001 (2007).

[56] C. D. Lu and K. Ukai, Branching ratios of $B \to D(s)K$ decays in perturbative QCD approach, Eur. Phys. J. C **28,** 305 (2003).

[57] J. Beringer *et al.* (Particle Data Group), Review of particle physics (RPP), Phys. Rev. D **86,** 010001 (2012).

[58] R. H. Li, C. D. Lu, and H. Zou, The $B(B_s) \to D_{(s)}P, D_{(s)}V, D_{(s)}^*P$ and $D_{(s)}^*V$ decays in the perturbative QCD approach, Phys. Rev. D **78,** 014018 (2008).

[59] H. Y. Cheng and C. K. Chua, QCD factorization for charmless hadronic B_s decays revisited, Phys. Rev. D **80,** 114026 (2009).

[60] A. L. Kagan, Polarization in $B \to VV$ decays, Phys. Lett. B **601,** 151 (2004).

[61] J. G. Korner and G. R. Goldstein, Quark and particle helicities in hadronic charmed particle decays, Phys. Lett. B **89,** 105 (1979).

[62] Y. Y. Keum, H. N. Li, and A. I. Sanda, Penguin enhancement and $B \to K\pi$ decays in perturbative QCD, Phys. Rev. D **63,** 054008 (2001).

[63] J. L. Beuzit, D. Segransan, T. Forveille, S. Udry, X. Delfosse, M. Mayor, C. Perrier, M. C. Hainaut, C. Roddier, F. Roddier *et al.*, New neighbours. 3. 21 new companions to nearby dwarfs, discovered with adaptive optics, Astron. Astrophys. **425,** 997 (2004).